Multi-curvature liquid meniscus in a nanochannel: Evidence of interplay between intermolecular and surface forces†

Pilnam Kim,[a] Ho-Young Kim,[ab] Jae Kwan Kim,[a] Günter Reiter[c] and Kahp Y. Suh*[ab]

Received 9th June 2009, Accepted 21st August 2009
First published as an Advance Article on the web 17th September 2009
DOI: 10.1039/b911271e

We examined the formation of a multiply curved meniscus inside rectangular nanochannels, whose width ranges from 50 to 800 nm at a constant height of 200 nm. When the channel width is smaller than ~400 nm under partial wetting conditions, a distinct multi-curvature meniscus was observed at the advancing front with an edge disjoined from the wall. In contrast, a typical pre-wetting film was observed at the front regardless of the channel size for complete wetting conditions. Our theoretical analysis demonstrated that the multi-curvature meniscus is generated from the increased contribution of an extra pressure due to intermolecular interactions near the wall. In particular, a plug-like meniscus profile was observed at the advancing liquid front for the 50 nm wide channel owing to an overlap between convex curvatures at the channel walls. Finally, we showed that the filling velocity of liquid can be decreased by decreasing the channel size due to the reduced wettability.

Introduction

An important branch of nanofluidics research is to reveal the dynamic aspects of wetting and flowing of a liquid in nanoscale channels or pores.[1–5] Despite increasing demands for understanding of liquid flow in nanochannels, how a liquid wets the surface of nanochannel or nanopore[1,3] is still far from clear, in part due to difficulty in fabricating a well-defined nanochannel[6] and visualizing distinct meniscus profiles. When the three phases of liquid/gas/solid meet, a meniscus is formed whose shape is determined by an equilibrium contact angle of θ_{eq}. On a macroscopic scale, this meniscus formation and related static wetting phenomena can be well described by the Young–Laplace equation. On a nanoscopic scale, however, long-range intermolecular interactions (*e.g.*, dispersion forces like van der Waals forces) across the channel come into play and become significant as compared to surface tension forces, thereby altering the meniscus shape and related wetting properties of a liquid.[7,8] Several researchers demonstrated the use of one-dimensional plate-type nanochannels[2,9] and carbon nanotubes[3] to observe a marching meniscus profile of water. In addition, molecular dynamics (MD) simulations involving millions of molecules have been employed to understand dynamic aspects of liquid flow inside a nanoscale confined system. Deviations from classical predictions have been reported, such as a significant fluctuation of the density profile across the channel direction and an increased contribution from long range intermolecular forces near the solid wall.[10–13] To elucidate the interplay between intermolecular and surface forces and the resulting wetting properties of a liquid within a nanochannel, however, a more systematic study by using nanochannels with varying dimensions would be of great benefit.

Here we report on the formation and shape-changes of a meniscus inside a nanochannel. For the channel fabrication, homogeneous (*i.e.*, all channel walls are made from the same material) and heterogeneous channels were considered. First, homogeneous, rectangular nanochannels of polymer (polyurethane acrylate, PUA) were fabricated by reversibly sealing a top channel layer onto a bottom layer with the aid of electrostatic attraction (so called, reversibly bonded nanochannels, RBNs).[14] Second, heterogeneous, rectangular nanochannels of the same polymer were formed on gold substrate using the same method. Into these channels, a low-viscosity liquid prepolymer (Novolac Optical Adhesive, NOA or polyethylene glycol diacrylate, PEG-DA) was introduced by capillarity-driven flow. This prepolymer was subsequently photo-crosslinked to permanently fix the shape of a meniscus which was then measured by scanning electron microscopy (SEM) after removal of the channel mold from the substrate. The dimensions of the nanochannels ranged from 50 nm to 800 nm in width at a fixed height of 200 nm. This approach for observing the capillary imbibition was previously demonstrated in a method called "micromolding in capillaries" (MIMIC) using an elastomeric mold such as polydimethylsiloxane (PDMS).[15] For nanochannels, it is difficult to achieve the sub-100 nm features due to low tensile modulus (~1.8 MPa) of the PDMS. Several researchers have reported that PDMS suffers from deformation, buckling, or collapse of small features when peeled from the original master.[16] The key advantage of the method introduced here, therefore, is the formation of reversibly sealed nanochannels by spontaneous attachment of a well-defined, high-resolution PUA nanochannel onto a bottom layer (*i.e.*, the substrate, either PUA or gold) in a highly reproducible manner.[14]

[a]*School of Mechanical and Aerospace Engineering, Seoul National University, Seoul, 151-742, Korea. E-mail: sky4u@snu.ac.kr*
[b]*Institute of Advanced Machinery and Design, Seoul National University, Seoul, 151-742, Korea*
[c]*Institute of Physics, University of Freiburg, 79104 Freiburg, Germany*
† Electronic supplementary information (ESI) available: Supplemental Figures S1–S5. See DOI: 10.1039/b911271e

Methods and materials

Preparation of top channel mold and channel bonding

A small amount (~0.1–0.5 mL) of UV curable PUA (polyurethane acrylate) was drop-dispensed on a silicon master and the supporting poly(ethylene terephthalate) (PET) film was carefully placed on top of the surface to make conformal contact. The PET film used in this study was surface modified with urethane groups to increase adhesion to the acrylate-containing monomer (Minuta Tech. Korea). The silicon master had been prepared by photolithography or electron-beam lithography depending on the feature size. To cure, the sample was exposed to UV (250–356 nm) for 3 sec at an intensity of 90 mW/cm^2 after adding 1 wt% of the UV initiator (2,2-dimethoxy-2-phenylacetophenone, Aldrich) with respect to the amount of polymer. After UV curing, the fabricated PUA mold was peeled off from the master using sharp tweezers. Details on the fabrication of reversibly bonded nanochannels (RBNs) can be found elsewhere.[14]

Capillarity-driven flow inside nanochannels

The RBNs were used for flowing a low-viscosity UV-curable liquid prepolymer: Norland Optical Adhesive, NOA 71 (viscosity $\sim$ 200 cp) and polyethylene glycol diacrylate, PEG-DA ($M_w = 256$, viscosity $\sim$ 20 cp). For this experiment, both ends of the mold were cut such that the prepolymer spontaneously filled inside the channels. After capillary filling, the filled prepolymer was exposed to UV for 3 sec and the mold was removed using a sharp tweezer, leaving behind a polymer replica without a residual layer.

Scanning electron microscopy (SEM) measurements

Images were taken using high-resolution SEM (XL30FEG, Philips Electron Co., Netherlands) at an acceleration voltage higher than 5 kV. Samples were coated with a 10 nm Au layer prior to analysis to prevent charging.

Measurements of contact angle and capillary filling rate

Advancing contact angles were measured with a Ramé-Hart goniometer (Mountain Lakes) equipped with a video camera. Reported values represent averages of at least 6 independent measurements. The flow rates inside the nanochannels were recorded and analyzed with a high-speed CCD camera (Nac Corp., Hi-Dcam PCI) connected to an optical microscope (Olympus, IX71).

Results and discussion

Observation of the meniscus in rectangular nanochannels

Fig. 1a shows a schematic illustration of the capillarity-driven filling of a liquid inside homogeneous RBNs made of PUA and an illustration of the formation of asymmetric menisci within a channel (see Supplemental methods for details and Supplemental Figure S1 in the ESI).† The PUA channel was made by an electrostatic-assisted contact with the PUA layer that had been spin-coated on a flexible polyethylene terephthalate (PET) film

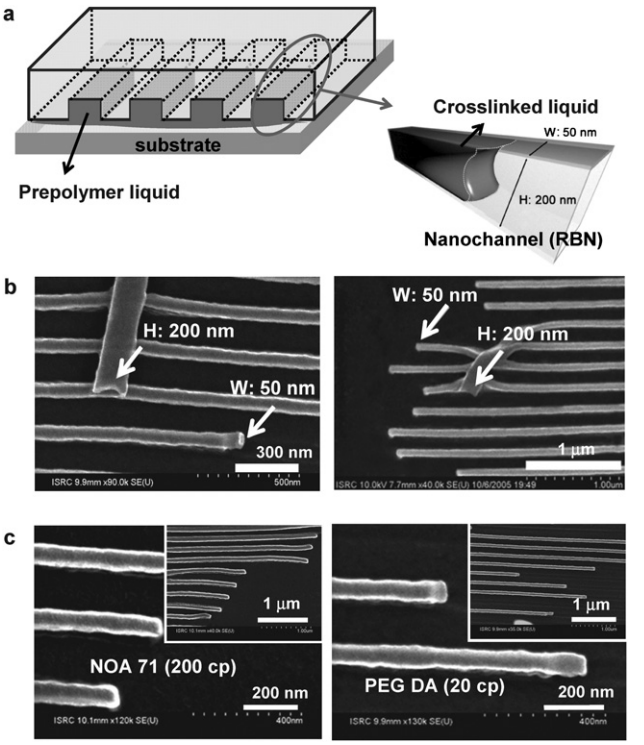

Fig. 1 A schematic illustration of experiment and SEM images of multi-curvature of meniscus. a, A schematic illustration for the formation of asymmetric menisci within the channel. b, SEM images showing the crosslinked nanostrips using PEG-DA. As judged by the delaminated nanostrips, asymmetric menisci were clearly found in the width and height directions. c, SEM images showing the effects of viscosity on the shape of a meniscus: NOA 71 (~200 cp) (left panel), PEG DA (~20 cp) (right panel). No notable difference in the shapes was observed between the two polymers. The nanochannel of 50 nm width and 200 nm height was used throughout this experiment.

substrate. Details on the fabrication of RBNs by electrostatic attraction can be found elsewhere.[14] The liquid prepolymer was applied at one side of the nanochannel system which was filled by capillarity-driven flow (Fig. 1a). The whole assembly was then exposed to UV for 3 seconds using a high-energy mercury lamp (90 mW/cm^2) at 10 cm distance. Fig. 1b–c shows examples of crosslinked polymer nanostructures formed by a capillarity-driven flow through nanochannels of 50 nm width and 200 nm height. For this experiment, two liquid prepolymers with similar surface tension ($\gamma_{LV} \sim 34$ mJ/m^2) were used: NOA 71 (viscosity, $\eta \sim 200$ cp) and PEG-DA (viscosity, $\eta \sim 20$ cp). The meniscus in the 50 nm width directions in Fig. 1b–c exhibited a plug-like profile, while a multi-curvature meniscus with a concave center was observed in the 200 nm height direction (as judged from delaminated nanostrips in Fig. 1b upon removal of the top channel mold). The fact that different meniscus profiles were found in the two directions strongly hints at a potential effect of channel dimension on the shape of the liquid meniscus. Moreover, as can be seen from the figure, no notable difference was observed between the two polymers. It suggests that viscosity is not a crucial factor for determining the shape of the meniscus.

Although a deformation of the meniscus has already been reported by Tas *et al.*,[2] nanochannels of a very low aspect ratio

(AR) of height/width ($\sim 10^{-2}$) were used in their study. In the case of channels capped by a thin layer, the negative pressure induced by capillarity resulted in a deflection of the thin capping layer, which, in turn, led to a deformation of the meniscus. This effect was strongly dependent on the width of the channel, and was only significant for channels with a small AR.[17] The use of rectangular channels with higher AR ($>10^{-1}$), thus, allows one to assume that such deflection was negligible in our system with a much thicker capping layer.

Wettability effect on the meniscus pattern in nanochannels

Based on the above observations, we hypothesize that the meniscus formation inside a nanochannel is not solely determined by the capillary effect observed at macroscopic scales. We consider that intermolecular forces across the channel and properties of the wall, such as roughness will become relevant. To date, the best-understood nanofluidic system involving intermolecular interaction is a thin liquid film that is supported on a solid substrate. The interplay between destabilizing long-range intermolecular force and stabilizing surface tension (Laplace pressure) in the thin liquid film is well understood.[18,19] One of the relevant parameters for describing the wetting behavior of a thin liquid film is the equilibrium spreading coefficient ($S_{eq} = \gamma_{SV} - \gamma_{SL} - \gamma_{LV} \equiv \gamma_{LV}(cos\,\theta_{eq} - 1)$). Here γ_{SV} is the surface tension of the solid substrate, and γ_{SL} and γ_{LV} are the solid/liquid and liquid/air interfacial tensions, respectively.[20] Also, Young's equation $\gamma_{LV}\,cos\,\theta_{eq} = \gamma_{SV} - \gamma_{SL}$ allows the relation of the interfacial tension to the equilibrium contact angle θ_{eq}.[21] Here S_{eq} is positive or almost zero for complete wetting, while S_{eq} is negative for partial wetting. If a liquid partially wets a solid surface ($S_{eq} < 0$), the liquid film is at best metastable and may rupture and dewet.

A comparable example is the formation of a pre-wetting film in the complete wetting regime ($S_{eq} > 0$). It is well known that in the complete wetting case an ultrathin pre-cursor film develops ahead of the meniscus wedge (ahead of the apparent contact line), whose thickness is typically in the order of nanometers.[5,20] In the partial wetting regime ($S_{eq} < 0$), on the other hand, such a pre-cursor film does not exist. Recognizing that an ultrathin layer is highly affected by intermolecular forces near the wall, we assume that the meniscus shape will also be modified close to the wall.[15]

To verify our hypothesis on the influence of the properties of the wall, control experiments have been carried out by using the homogenous and heterogeneous RBNs with the same prepolymer of NOA 71. Fig. 2 shows a schematic illustration of the multi-curvature menisci and corresponding SEM images for PUA channels on both gold (in panel a) and PUA substrates (in panel b), respectively. As can be seen from the figures, the meniscus shape was distinctly dependent on the wettability of the bottom substrate. For the PUA substrates (partial wetting), multi-curvature menisci were formed both in the width and height directions, in accordance with the results shown in Fig. 1. For the gold substrates (complete wetting), a thin pre-cursor film was formed on the gold substrate with multi-curved menisci only in the other three directions (see also Supplemental Fig. S2, ESI).† In this case, the pre-cursor film reached out as far as 1.5 μm ahead of the meniscus. These results suggest that the

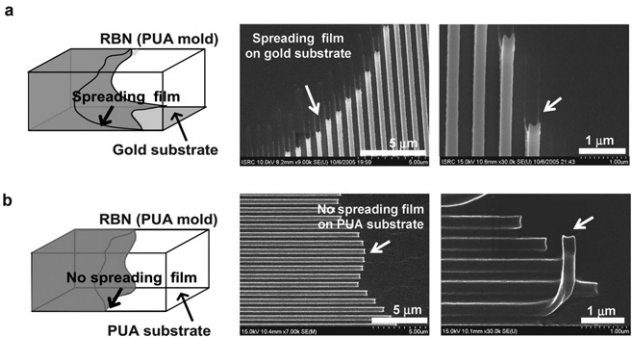

Fig. 2 Effects of wettability on the shape of a meniscus. Schematic illustration of the resulting multi-curvature menisci and corresponding SEM images within rectangular PUA nanochannels on (a) gold (complete wetting, $S_{eq} \sim 0$) and (b) PUA substrate (partial wetting, $S_{eq} < 0$), respectively. The nanochannel of 250 nm width and 200 nm height was used for this experiment.

multi-curvature meniscus presented here originated from partial wetting characteristics of the prepolymer and not from shrinkage during curing or other extrinsic effects.

Another notable finding is that the same multi-curvature meniscus forms on the polymer surface when a thermoplastic polymer melt was used instead of a UV-curable resin. For this experiment, a poly(methyl methacrylate) (PMMA) film was spin-coated on a silicon substrate. PMMA was pulled into the channels of a nanoscale mold (400 nm width, 800 nm height) by capillary action above the polymer's glass transition temperature (T_g = 105 °C) (Supplemental Fig. S3, ESI).† As expected, a similar multi-curvature meniscus was found on the advancing front of the polymer, suggesting that the wetting dynamics reported here can be equally applied to other polymers and general liquids in nanochannels. It is also noted that the shrinkage of polymer structure is negligible under the fast curing process reported here,[22] which corroborates an earlier study involving microscale liquid flow where no distortion in the cured structure was reported.[15]

Channel size effect on the shape of meniscus in nanochannels

In addition to the wettability of the channel walls by the liquid, the size of the channel is also expected to have an influence on the shape of the meniscus. To investigate this issue in a more systematic manner, we fabricated nanochannels with varying dimensions (50 nm–800 nm in width, 200 nm in height) and then introduced the low-molecular weight (M_w) PEG-DA prepolymer (M_w = 256) inside the channels. The resulting meniscus profiles were measured by using a SEM (Fig. 3a). The images on the left panel show a cross-sectional view of the PUA channel mold with geometrical description. The images on the right panel show a large-area and enlarged views of the filled nanostrips after UV-curing and mold removal. The advancing contact angle (θ_A) of this prepolymer on a smooth PUA substrate was measured to be about 43° (Supplemental Fig. S4a, ESI),† so that the prepolymer can be spontaneously driven into the nanochannels by capillarity. Interestingly, multi-curvature menisci were observed throughout the channels tested. For the channel width of 800 nm or larger, this meniscus deformation was not easily recognizable

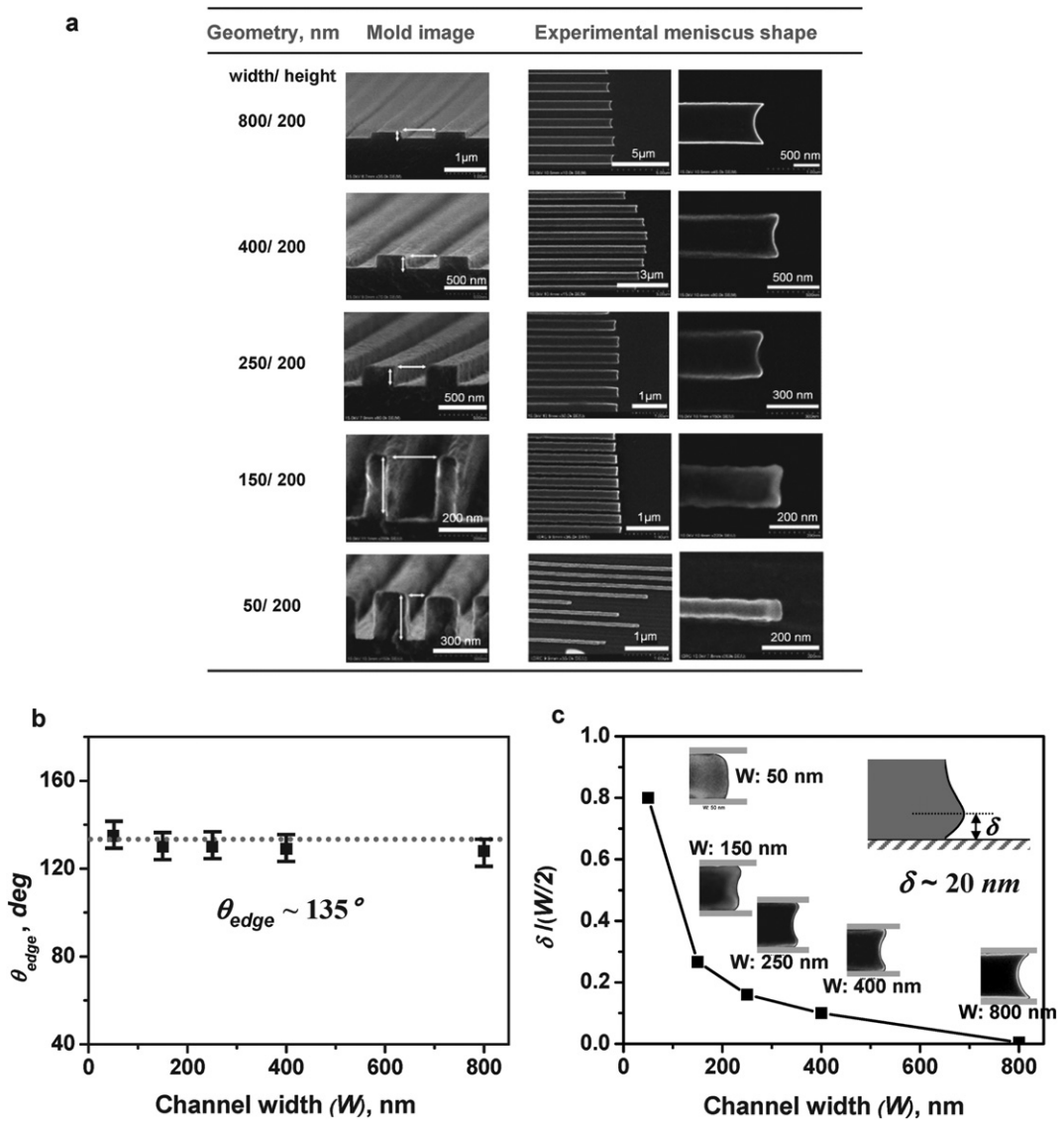

Fig. 3 Effects of channel size on the shape of a meniscus. a, SEM images of the rectangular PUA channel molds with width ranging from 800 nm to 50 nm (left panel) and the corresponding large-area and magnified views of meniscus within the channel (right panel). Note that the molds showed well-defined edge profiles. b, Plot of the apparent edge contact angle (θ_{edge}) with channel width based on the analysis of SEM images. c, Plot of the distance δ normalized by half of the channel width W. The inset images show the definition of δ and representative SEM images for each channel. Note that the formation of a multi-curvature meniscus is more pronounced with decreasing channel width.

but a careful examination at locations close to the wall of the mold revealed a slight distortion of the meniscus. For the channel width of 400 nm or less, multi-curved menisci were readily detected. It is worth noting that the meniscus shape in the height direction (200 nm) was the same regardless of the variation in width. This shape was similar to that in the width direction of the 250 nm wide channel (Fig. 3a).

Here, we define the characteristic distance (δ) of a layer next to the wall, illustrated in Fig. 3c, as the distance from the wall at which a meniscus deviated from its original single-curvature meniscus shape. To analyze the meniscus profile, each meniscus was plotted with the best-fitting curve and the resulting curves were drawn with LABVIEW (Supplemental Fig. S5, ESI).† For simplicity, both axes were normalized with the channel width, W. According to image analysis, θ_{edge} was ~135° and δ was ~20 nm for the nanochannels used in the experiment (Fig. 3b–c). Consequently, with a characteristic distance of $\delta \sim 20$ nm from both sides of a 50 nm channel we obtained roughly overlap of the meniscus profiles close to the walls, yielding at the advancing front a plug-like profile without any notable curvature (Fig. 3a).

To explain the formation of a multi-curvature meniscus, we start with the simple geometrical analysis of the liquid interface. We derive a phenomenological model based on the Young–Laplace equation,[21] which relates the pressure drop across a liquid meniscus to its curvature:

$$\Delta P = \gamma\left(\frac{1}{r_h}+\frac{1}{r_w}\right) \quad (1)$$

where ΔP represents the difference between the pressure in the liquid, P_L, and the pressure in the vapor, P_∞, ($\Delta P = P_L - P_\infty$), γ

is the surface tension and, γ_h and γ_w are the radii of curvature for two different directions (H and W, respectively) of the meniscus. The radius of curvature is taken as negative (positive) for a concave (convex) curvature of the liquid surface. For a position denoted cc in Fig. 4a of a rectangular channel, we can therefore write:

$$P_L - P_\infty = -\gamma\left(\frac{2\cos\theta_{cc}}{H} + \frac{2\cos\theta_{cc}}{W}\right) \quad (2)$$

where θ_{cc} represents the contact angle at the position cc. The presence of a layer of thickness δ near the wall can be interpreted in terms of competition between long and short range forces. We consider the effective pressure, P_{eff}, which includes the macroscopic Laplace pressure, P_L, and extra disjoining pressure, Π: $P_{eff} = P_L + \Pi$. Here Π represents an additional pressure in the thin liquid flow, which originated from intermolecular interactions near the wall. As shown in Fig. 4b and 4c, the extra pressure Π is considerable near the wall, while the Laplace pressure P_L should be constant at all positions. Thus, the augmented Young–Laplace equation at the position denoted by ce is:

$$P_{eff} - P_\infty = P_L + \prod - P_\infty = -\gamma\left(\frac{2\cos\theta_{ce}}{H} - \kappa_{ce}\right) \quad (3)$$

where θ_{ce} are the contact angle at the position ce. κ_{ce} is related to the shape of the meniscus at the edge of channel. Combining eqs 2 and 3 gives an expression for the additional pressure Π at the position ce:

$$\prod = -\gamma\left(-\kappa_{ce} - \frac{2\cos\theta_{cc}}{W}\right) = \gamma(\kappa_{ce} - \kappa_{cc}) \quad (4)$$

where κ_{cc} is negative for hydrophilic channels. Thus, the extra pressure Π is expressed by the relation between the edge-curvature and the center-curvature. The negative value for Π represents a stable meniscus with a wedge-like profile (edge contact angle, θ_{edge} < bulk advancing contact angle, θ_A), leading to a pre-spreading film ($\kappa_{ce} < 0$). On the contrary, when $\Pi > 0$, a convex curvature is formed ($\kappa_{ce} > 0$) at the edge, implying that there exists a significant deformation of the meniscus or edge dewetting. For a 50 nm width channel, with a radius of convex curvature (w_{ce}) of ~19.5 nm and an edge-contact angle (θ_{edge}) of 135°, eq 4 predicts an extra pressure Π of ~20 bar. Competition of this pressure effect with the Laplace pressure based on the macroscopic contact angle $\Delta P = 12$ bar explains that the curvature of the liquid meniscus at the edge can be inverted, as shown Fig. 3a. This experimentally obtained extra pressure accounts for all the intermolecular interactions close to the channel wall.

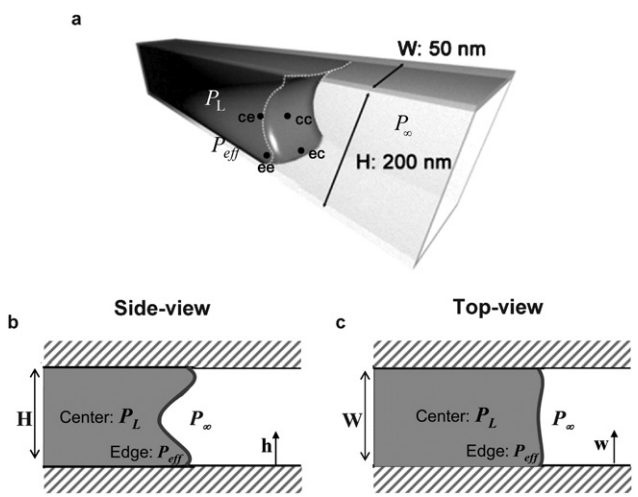

Fig. 4 Schematic illustrations of a multi-curvature meniscus in a rectangular nanochannel. a, Representation of a multi-curvature meniscus in a rectangular nanochannel with 50 nm width and 200 nm height, where P_L and P_∞, are the capillary pressure and vapor pressure, respectively. The effective pressure P_{eff} accounts for intermolecular interactions near the wall. b, Schematic illustration of meniscus shape at position center (c) and edge (e), side view of channel. c, Schematic illustration of meniscus shape at position center (c) and edge (e), top view of channel (50 nm width).

Analysis of capillary filling kinetics in nanochannels

In the following, we examine the effect of such multi-curvature menisci on the filling kinetics. We performed the measurement of the capillary filling speed of liquid in rectangular nanochannels with variable widths (800 nm, 250 nm, and 50 nm) at a constant channel height of 200 nm. The viscosity-dominant imbibition velocity in the channels is classically given by the well-known Lucas–Washburn–Rideal (LWR) equation.[23]

$$x = \left(\frac{R\gamma_{LV}\cos\theta}{2\eta}t\right)^{1/2} \quad (5)$$

where R is the hydraulic radius defined as the ratio of the cross-sectional area to the wetted perimeter of the channel. Shown in Fig. 5a are theoretical predictions from eq 5 (dot lines) and the experimentally measured (solid lines and symbols) imbibition length of liquid (PEG-DA) in nanochannels having three different widths. For the value of contact angle θ one typically takes the advancing contact angle θ_A, which was 43° for PEG-DA on the PUA substrate (see Supplemental Fig. 4a, ESI).† Although the filling dynamics obeyed the predicted $\sqrt{t}$-dependence, the actual velocity was slower than the expected value. Interestingly, we found different degrees of velocity reduction, ~8.5%, 19.6%, and 28.8% for W of 800 nm, 250 nm, and 50 nm, respectively. Our results indicate that the reduced filling speed is originated from deformation of the meniscus which could be represented by an increased value of the advancing contact angle (apparent advancing contact angle, $\theta_{A,app}$). As shown in Fig 5b, $\theta_{A,app}$ increased as the channel width decreased, which is caused by the increased contribution from intermolecular forces near the wall.

A reduced filling speed in nanochannels was reported previously by others,[2,24,25] which was attributed to various effects such as electroviscosity, increased fluid viscosity, and channel geometry due to negative pressure induced in the capillary. In our device, as described above, there is no effect of negative pressure induced by capillarity. Electroviscosity is not possible because we used a non-polar liquid. Our experiments, therefore, revealed the effect of the intermolecular interactions of liquid–solid–vapor, which lead to not only reduced pressure difference (ΔP) but reduced wettability of liquid. That is, an extra disjoining pressure generated from intermolecular forces leads to an increase in apparent advancing contact angle in the case of a metastable

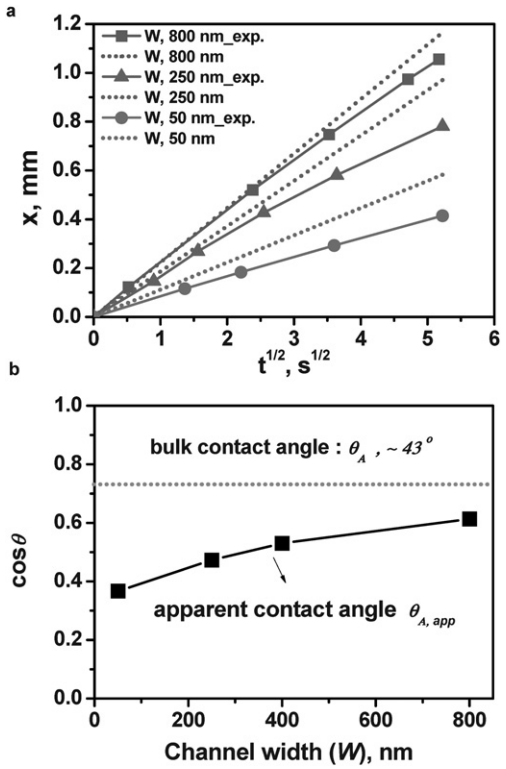

Fig. 5 Effects of channel dimension on filling velocity. a, Plot of the measured position of the moving meniscus (x) as a function of $t^{1/2}$ for filling of 800 nm, 250 nm, and 50 nm wide nanochannels with PEG-DA (solid lines with symbols) and the position of the filling front for the three channels expected by the Lucas–Washburn–Rideal (LWR) equation using the macroscopically measured advancing contact angle (dotted lines). b, dependence on the channel width (W) for the apparent advancing contact angle of liquid flowing inside nanochannels. $\theta_{A,app}$ is the contact angle fitted to measured channel filling data using the Lucas–Washburn–Rideal (LWR) equation (eq 5).

state (partially wetting liquid on surface). One can also hypothesize that there is a "stagnant" layer at the wall presumably due to the presence of a surface roughness, resulting in a retarded capillary flow by mechanical "pinning". A future study would be required to elucidate an exact origin of the retarded capillary flow using different surface roughness, material properties (wettability and surface tension), and channel geometry.

Conclusions

We have presented wetting properties of a liquid prepolymer inside nanochannels with varying widths from 50 to 800 nm for a constant height of 200 nm. Since the liquid is non-polar and non-volatile, we only had to consider the contributions from intermolecular and surface forces, while excluding contributions from segregation, thermal fluctuations, or electrical double layers. In the case of a liquid on a completely wettable channel wall, a pre-cursor film was formed ahead of the front of the meniscus, whereas a meniscus with a convex curvature (radius ~20 nm, edge contact angle ~135°) formed near the wall regardless of the channel size when the liquid partially wetted the channel wall.

We have also explored some consequences of these phenomena. The multi-curvature meniscus reconstructs due to the increased contribution of an extra pressure due *e.g.* to intermolecular interactions near the wall. Owing to an overlap between convex curvatures at the channel walls, a plug-like meniscus profile was observed at the advancing liquid front within the 50 nm wide channel. It indicates that the positive extra pressure near the wall (unstable condition comparable to dewetting) was high enough to deform the macroscopically observed single-curvature meniscus. Moreover, we showed that a reduction of filling velocity of liquid – enhanced with decreasing channel size – was caused by the reduced wettability.

Acknowledgements

This work was supported by the Korea Science and Engineering Foundation (KOSEF) grant (R01-2007-000-20675-0) and the Korean Research Foundation Grant funded by the Korean Government (MOEHRD) (KRF-2007-412-J03000). This work was supported in part by the WCU (World Class University) program (R31-2008-000-10083-0) and the Korea Research Foundation Grant funded by the Korean Government (MOEHRD) (Grant KRF-J03000).

References

1 S. Supple and N. Quirke, *Phys. Rev. Lett.*, 2003, **90**, 214501.
2 N. R. Tas, P. Mela, T. Kramer, J. W. Berenschot and A. van den Berg, *Nano Lett.*, 2003, **3**, 1537–1540.
3 M. P. Rossi, H. H. Ye, Y. Gogotsi, S. Babu, P. Ndungu and J. C. Bradley, *Nano Lett.*, 2004, **4**, 989–993.
4 A. Gunther and K. F. Jensen, *Lab Chip*, 2006, **6**, 1487–1503.
5 M. Rauscher and S. Dietrich, *Annu. Rev. Mater. Res.*, 2008, **38**, 143–172.
6 D. Mijatovic, J. C. T. Eijkel and A. van den Berg, *Lab Chip*, 2005, **5**, 492–500.
7 J. C. T. Eijkel and A. van den Berg, *Lab Chip*, 2005, **5**, 1202–1209.
8 J. Eijkel, *Lab Chip*, 2007, **7**, 299–301.
9 J. T. Cheng and N. Giordano, *Phys. Rev. E: Stat., Nonlinear, Soft Matter Phys.*, 2002, **65**, 031206.
10 X. J. Fan, N. Phan-Thien, N. T. Yong and X. Diao, *Phys. Fluids*, 2002, **14**, 1146–1153.
11 K. P. Travis and K. E. Gubbins, *J. Chem. Phys.*, 2000, **112**, 1984–1994.
12 K. P. Travis, B. D. Todd and D. J. Evans, *Phys. Rev. E: Stat., Nonlinear, Soft Matter Phys.*, 1997, **55**, 4288–4295.
13 X. Y. Chen, Y. Liu and J. M. Yang, *Mod. Phys. Lett. B*, 2008, **22**, 2649–2658.
14 P. Kim and K. Y. Suh, *Langmuir*, 2007, **23**, 4549–4553.
15 E. Kim and G. M. Whitesides, *J. Phys. Chem. B*, 1997, **101**, 855–863.
16 E. Delamarche, H. Schmid, B. Michel and H. Biebuyck, *Adv. Mater.*, 1997, **9**, 741–746.
17 J. W. van Honschoten, M. Escalante, N. R. Tas and M. Elwenspoek, *J. Colloid Interface Sci.*, 2009, **329**, 133–139.
18 J. A. N. Zasadzinski, J. B. Sweeney, H. T. Davis and L. E. Scriven, *J. Colloid Interface Sci.*, 1987, **119**, 108–116.
19 H. Wong, S. Morris and C. J. Radke, *J. Colloid Interface Sci.*, 1992, **148**, 317–336.
20 P. G. de Gennes, *Rev. Mod. Phys.*, 1985, **57**, 827–863.
21 T. Young, *Philos. Trans. R. Soc. London*, 1805, **95**, 65–87.
22 D. L. Kurdikar and N. A. Peppas, *Polymer*, 1995, **36**, 2249–2255.
23 D. Mayers, *Surfaces, Interfaces, and Colloids*, VCH, New York, 1991.
24 K. M. van Delft, J. C. T. Eijkel, D. Mijatovic, T. S. Druzhinina, H. Rathgen, N. R. Tas, A. van den Berg and F. Mugele, *Nano Lett.*, 2007, **7**, 345–350.
25 D. Geromichalos, F. Mugele and S. Herminghaus, *Phys. Rev. Lett.*, 2002, **89**, 104503.

